Journal of Computational Physics 318 (2016) 110–121

Contents lists available at ScienceDirect

Journal of Computational Physics

www.elsevier.com/locate/jcp

Short note

A new fifth order finite difference WENO scheme for solving hyperbolic conservation laws ☆

Jun Zhu [a], Jianxian Qiu [b,*]

[a] College of Science, Nanjing University of Aeronautics and Astronautics, Nanjing, Jiangsu 210016, PR China
[b] School of Mathematical Sciences and Fujian Provincial Key Laboratory of Mathematical Modeling and High-Performance Scientific Computing, Xiamen University, Xiamen, Fujian 361005, PR China

ARTICLE INFO

Article history:
Received 16 April 2016
Received in revised form 2 May 2016
Accepted 3 May 2016
Available online 7 May 2016

Keywords:
Fifth order WENO scheme
Hyperbolic conservation laws
Finite difference framework

ABSTRACT

In this paper a new simple fifth order weighted essentially non-oscillatory (WENO) scheme is presented in the finite difference framework for solving the hyperbolic conservation laws. The new WENO scheme is a convex combination of a fourth degree polynomial with two linear polynomials in a traditional WENO fashion. This new fifth order WENO scheme uses the same five-point information as the classical fifth order WENO scheme [14,20], could get less absolute truncation errors in L^1 and L^∞ norms, and obtain the same accuracy order in smooth region containing complicated numerical solution structures simultaneously escaping nonphysical oscillations adjacent strong shocks or contact discontinuities. The associated linear weights are artificially set to be any random positive numbers with the only requirement that their sum equals one. New nonlinear weights are proposed for the purpose of sustaining the optimal fifth order accuracy. The new WENO scheme has advantages over the classical WENO scheme [14,20] in its simplicity and easy extension to higher dimensions. Some benchmark numerical tests are performed to illustrate the capability of this new fifth order WENO scheme.

1. Introduction

Recently, many high order finite difference or finite volume numerical methods have been investigated to solve for hyperbolic conservation laws. The essentially non-oscillatory (ENO) and weighted ENO (WENO) schemes, which have been applied quite successfully to solve the problems with strong shocks, contact discontinuities and sophisticated smooth structures, are the primary schemes used as the current state of the art in the literature. For the purpose of achieving uniform high order accuracy both in space and time, Harten and Osher [11] gave a weaker version of the total variation diminishing (TVD) criterion [8] and on which they established a basis for the reconstruction of high order ENO type schemes. And a series of ENO schemes were developed by Harten et al. [10] to solve one dimensional problems. The most crucial spirit of these ENO type schemes is to apply the smoothest candidate stencil among all stencils to approximate the variables at cell boundaries for the sake of sustaining high order accuracy in smooth region and not introducing spurious oscillations in nonsmooth region [21,22]. The first WENO scheme was originally proposed by Liu, Osher and Chan [15], in which instead of using the optimal smooth candidate stencil, a linear convex combination of all stencils including nonsmooth stencils is used. After that, such WENO scheme was improved by Jiang and Shu [14], in which a general framework for the designing

☆ The research is partly supported by NSFC grants 11372005, 11571290 and 91530107.
* Corresponding author.
E-mail addresses: zhujun@nuaa.edu.cn (J. Zhu), jxqiu@xmu.edu.cn (J. Qiu).

http://dx.doi.org/10.1016/j.jcp.2016.05.010
0021-9991/

of new smoothness indicators and nonlinear weights was specified in detail. For the system case, the WENO schemes are based on local characteristic decomposition and numerical flux splitting method to avoid spurious oscillations nearby strong shocks or contact discontinuities. And some other famous WENO schemes are proposed for specifical computation needs, such as optimized WENO schemes for solving linear waves with discontinuity [23], monotonicity preserving WENO schemes for very high order accuracy simulation [2], hybrid compact WENO schemes for computing shock and turbulence interaction [17,18], and robust WENO schemes for dealing with distorted local mesh geometry or the degeneration of the mesh quality varies for complex computational domain [12,16,19] etc. The various types of ENO and WENO schemes [4,5,9,13–15,21,22,25] are quite successful in numerical simulations for steady and unsteady problems harboring strong discontinuities and sophisticated smooth structures.

Comparing with the above mentioned literature, especially including classical WENO schemes proposed by Jiang and Shu [14,20], the major advantages of the new finite difference fifth order WENO scheme in this paper are its simplicity, high order accuracy and easy implementation in the computation. This new WENO scheme has a convex combination of a fourth degree polynomial which should subtract other two linear polynomials by multiplying proper constant parameters, then compound these three unequal degree polynomials which use information on different spatial stencils in a WENO type methodology including artificially setting linear weights for the conservation without losing numerical accuracy, computing smoothness indicators and proposing new nonlinear weight formula which is different to the expression specified in [3,6], for solving the Euler equations in one and two dimensions. The essential merits of such methodology are its simplicity in space by the definition of positive linear weights, and only one five-point stencil and two two-point stencils are used to reconstruct three different degree polynomials. An innovation of modifying the fourth degree polynomial is very essential for sustaining the scheme's high order accuracy, otherwise, some traditional robust WENO methodologies will degrade their numerical accuracy to a lower order of accuracy. Therefore, we try to use fifth order approximation to the numerical flux for simplicity and easy implementation for the sake of obtaining high order accuracy in smooth region, and switch it to either of two second order approximations on smaller spatial stencils when the computing field is adjacent the shock or contact discontinuities for the sake of avoiding spurious oscillations. Thereafter, the new nonlinear weight formulas are presented for the final high order numerical flux approximation procedure. When a large, centered stencil permits optimal stability and accuracy to be reached, this method will certainly reach that stability and accuracy. However, when the solution on that stencil is rough, it is beneficial to seek out a smaller TVD-like stencil. The two small stencils that are used ensure that (when the large stencil may be ignored) the method is effectively a TVD scheme with a van Albada-like limiter. Consequently, for non-smooth solution vector, this scheme operates like a TVD scheme with all the attendant stability properties of a TVD scheme. In other words, the fact that a TVD-like property is built into the method makes it closer to a Monotonicity Preserving WENO than a pure WENO-JS (which always relies on an ensemble of large stencils). All in all, the innovations of this paper lie in three aspects: the new way of reconstructing a modified fourth degree polynomial by subtracting two linear polynomials with proper parameters, a novel WENO type communication among three unequal (modified) polynomials for high accurate approximations in smooth region and non-oscillation in nonsmooth region, and the new manner of obtaining associated nonlinear weights.

The organization of the paper is as follows: in Section 2, we construct the new finite difference fifth order WENO scheme in detail. In Section 3, some classical numerical tests are presented to verify the numerical accuracy and efficiency of the new WENO scheme. Concluding remarks are given in Section 4.

2. New simple WENO scheme

One dimensional hyperbolic conservation laws is

$$\begin{cases} u_t + f_x(u) = 0, \\ u(x,0) = u_0(x), \end{cases} \tag{2.1}$$

and the associated semidiscretization of (2.1) can be reformulated as

$$\frac{du}{dt} = L(u), \tag{2.2}$$

where $L(u)$ is the high order spatial discrete formulation of $-f_x(u)$. For simplicity, the uniform mesh is distributed into some cells $I_i = [x_{i-1/2}, x_{i+1/2}]$, with the uniform cell size is denoted as $x_{i+1/2} - x_{i-1/2} = h$ and associated cell centers are defined as $x_i = \frac{1}{2}(x_{i+1/2} + x_{i-1/2})$. $u_i(t)$ is defined as a nodal point value $u(x_i, t)$. Therefore the right hand side of (2.2) can be reformulated as

$$L(u_i(t)) = -\frac{1}{h}(\hat{f}_{i+1/2} - \hat{f}_{i-1/2}), \tag{2.3}$$

where $\hat{f}_{i+1/2}$ is a numerical flux which has a fifth order approximation of flux $f(u)$ at the boundary $x_{i+1/2}$ of target cell I_i in this paper. If the numerical flux $\hat{f}_{i+1/2}$ is taken into account the fifth order approximation, then $\frac{1}{h}(\hat{f}_{i+1/2} - \hat{f}_{i-1/2})$ is the fifth order approximation to $f_x(u)$ at $x = x_i$. For an ordinary flux $f(u)$, it can be split into $f(u) = f^+(u) + f^-(u)$, satisfying $\frac{df^+(u)}{du} \geq 0$ and $\frac{df^-(u)}{du} \leq 0$. A simplest Lax–Friedrichs splitting is applied as $f^{\pm}(u) = \frac{1}{2}(f(u) \pm \alpha u)$, in which α is set as

$\max_u |f'(u)|$ over the whole range of u. The detailed flowchart of the new simple fifth order WENO scheme is described as follows, for simplicity, we only do the reconstruction of $f^+(u)$ at point $x_{i+1/2}$ and denote it as $\hat{f}^+_{i+1/2}$.

Step 1. Choose the following big stencil: $T_1 = \{I_{i-2}, I_{i-1}, I_i, I_{i+1}, I_{i+2}\}$. It is easy to obtain a fourth degree reconstructed polynomial $p_1(x)$ which is based on the nodal point information of the flux splitting and satisfying:

$$\frac{1}{h}\int_{x_j-h/2}^{x_j+h/2} p_1(x)dx = f_j^+,\ j = i-2, i-1, i, i+1, i+2. \tag{2.4}$$

Its explicit expression is same as specified in [1]

$$\begin{aligned} p_1(x) = f_i^+ &+ \frac{-82f_{i-1}^+ + 11f_{i-2}^+ + 82f_{i+1}^+ - 11f_{i+2}^+}{120}(\frac{x-x_i}{h}) + \\ &\frac{40f_{i-1}^+ - 3f_{i-2}^+ - 74f_i^+ + 40f_{i+1}^+ - 3f_{i+2}^+}{56}((\frac{x-x_i}{h})^2 - \frac{1}{12}) + \\ &\frac{2f_{i-1}^+ - f_{i-2}^+ - 2f_{i+1}^+ + f_{i+2}^+}{12}((\frac{x-x_i}{h})^3 - \frac{3}{20}(\frac{x-x_i}{h})) + \\ &\frac{-4f_{i-1}^+ + f_{i-2}^+ + 6f_i^+ - 4f_{i+1}^+ + f_{i+2}^+}{24}((\frac{x-x_i}{h})^4 - \frac{3}{14}(\frac{x-x_i}{h})^2 + \frac{3}{560}). \end{aligned} \tag{2.5}$$

Choose another two smaller stencils: $T_2 = \{I_{i-1}, I_i\}$ and $T_3 = \{I_i, I_{i+1}\}$. It is also very easy for us to get the two linear polynomials which are based on the nodal point information of the flux splitting and satisfying

$$\frac{1}{h}\int_{x_j-h/2}^{x_j+h/2} p_2(x)dx = f_j^+,\ j = i-1, i, \tag{2.6}$$

and

$$\frac{1}{h}\int_{x_j-h/2}^{x_j+h/2} p_3(x)dx = f_j^+,\ j = i, i+1. \tag{2.7}$$

Their explicit expressions are

$$p_2(x) = f_i^+ + (f_i^+ - f_{i-1}^+)(\frac{x-x_i}{h}), \tag{2.8}$$

and

$$p_3(x) = f_i^+ + (f_{i+1}^+ - f_i^+)(\frac{x-x_i}{h}). \tag{2.9}$$

Step 2. The main selection principle of the linear weights is solely based on the consideration of a balance between accuracy and ability to achieve essentially nonoscillatory shock transitions. In all of our numerical tests, following the practice in [7,26], we take the positive linear weights as $\gamma_1 = 0.98$ and $\gamma_2 = \gamma_3 = 0.01$. The linear weights can be chosen to be any set of positive numbers with the condition that the summation is one and would not pollute the new scheme's optimal accuracy.

Step 3. Compute the smoothness indicators $\beta_n,\ n = 1, 2, 3$, which measure how smooth the functions $p_n(x),\ n = 1, 2, 3$, are in the target cell I_i. The smaller these smoothness indicators, the smoother the functions are in I_i. We use the same recipe for the smoothness indicators as in [1,14,20]

$$\beta_n = \sum_{\alpha=1}^{r}\int_{I_i} h^{2\alpha-1}(\frac{d^\alpha p_n(x)}{dx^\alpha})^2 dx,\ n = 1, 2, 3. \tag{2.10}$$

The associated explicit expressions are

$$\begin{aligned} \beta_1 = (&\frac{-82f_{i-1}^+ + 11f_{i-2}^+ + 82f_{i+1}^+ - 11f_{i+2}^+}{120} + \\ &\frac{2f_{i-1}^+ - f_{i-2}^+ - 2f_{i+1}^+ + f_{i+2}^+}{120})^2 + \end{aligned}$$

$$\frac{13}{3}\left(\frac{40f_{i-1}^{+}-3f_{i-2}^{+}-74f_{i}^{+}+40f_{i+1}^{+}-3f_{i+2}^{+}}{56}+\frac{123}{455}\frac{-4f_{i-1}^{+}+f_{i-2}^{+}+6f_{i}^{+}-4f_{i+1}^{+}+f_{i+2}^{+}}{24}\right)^2+\frac{781}{20}\left(\frac{2f_{i-1}^{+}-f_{i-2}^{+}-2f_{i+1}^{+}+f_{i+2}^{+}}{12}\right)^2+\frac{1421461}{2275}\left(\frac{-4f_{i-1}^{+}+f_{i-2}^{+}+6f_{i}^{+}-4f_{i+1}^{+}+f_{i+2}^{+}}{24}\right)^2, \tag{2.11}$$

$$\beta_2=(f_{i-1}^{+}-f_{i}^{+})^2, \tag{2.12}$$

and

$$\beta_3=(f_{i}^{+}-f_{i+1}^{+})^2. \tag{2.13}$$

The expansions of (2.11) to (2.13) in Taylor series about f_i^+ are obtained as

$$\beta_1=h^2((f_i^+)')^2+13h^4((f_i^+)'')^2/12+h^6(5467((f_i^+)''')^2-14(f_i^+)''(f_i^+)^{(4)}-336(f_i^+)'(f_i^+)^{(5)})/5040+O(h^8)=h^2((f_i^+)')^2(1+O(h^4))=O(h^2), \tag{2.14}$$

$$\beta_2=h^2((f_i^+)')^2-h^3(f_i^+)'(f_i^+)''+h^4\left(\frac{(f_i^+)''}{4}+\frac{(f_i^+)'(f_i^+)'''}{3}\right)+O(h^5)=h^2((f_i^+)')^2(1+O(h))=O(h^2), \tag{2.15}$$

and

$$\beta_3=h^2((f_i^+)')^2+h^3(f_i^+)'(f_i^+)''+h^4\left(\frac{(f_i^+)''}{4}+\frac{(f_i^+)'(f_i^+)'''}{3}\right)+O(h^5)=h^2((f_i^+)')^2(1+O(h))=O(h^2). \tag{2.16}$$

It is assumed that the indicators of smoothness can be rewritten as: $\beta_1=D(1+O(h^4))$ and $\beta_{2,3}=D(1+O(h))$, in which $D=h^2((f_i^+)')^2$ is a non-zero constant independent of n on condition that $(f_i^+)'\neq 0$.

Step 4. Calculate the non-linear weights based on the linear weights and the smoothness indicators. For instance, as shown in [3,6], we use new τ which is simply defined as the absolute deference between β_1, β_2 and β_3, and is different to the formula specified in [3,6]. Since the two difference expansions in Taylor series about f_i^+ are

$$\beta_1-\beta_2=(f_i^+)'(f_i^+)''h^3+\left(\frac{5((f_i^+)'')^2}{6}-\frac{(f_i^+)'(f_i^+)'''}{3}\right)h^4+O(h^5)=\begin{cases}O(h^3),\ (f_i^+)'\neq 0,\ (f_i^+)''\neq 0,\\ O(h^4),\ (f_i^+)'=0,\ (f_i^+)''\neq 0,\end{cases} \tag{2.17}$$

and

$$\beta_1-\beta_3=-(f_i^+)'(f_i^+)''h^3+\left(\frac{5((f_i^+)'')^2}{6}-\frac{(f_i^+)'(f_i^+)'''}{3}\right)h^4+O(h^5)=\begin{cases}O(h^3),\ (f_i^+)'\neq 0,\ (f_i^+)''\neq 0,\\ O(h^4),\ (f_i^+)'=0,\ (f_i^+)''\neq 0.\end{cases} \tag{2.18}$$

It is easy to verify

$$\tau=\left(\frac{|\beta_1-\beta_2|+|\beta_1-\beta_3|}{2}\right)^2=\begin{cases}O(h^6),\ (f_i^+)'\neq 0,\ (f_i^+)''\neq 0,\\ O(h^8),\ (f_i^+)'=0,\ (f_i^+)''\neq 0.\end{cases} \tag{2.19}$$

Then we define

$$\omega_n=\frac{\bar{\omega}_n}{\sum_{\ell=1}^{3}\bar{\omega}_\ell},\qquad \bar{\omega}_n=\gamma_n\left(1+\frac{\tau}{\varepsilon+\beta_n}\right),\quad n=1,2,3. \tag{2.20}$$

Here ε is a small positive number to avoid the denominator to become zero. By the usage of (2.14) to (2.16) and (2.19) in the smooth region, it satisfies

$$\frac{\tau}{\varepsilon+\beta_n}=O(h^4),n=1,2,3, \tag{2.21}$$

on condition that $\varepsilon \ll \beta_n$. Therefore, the nonlinear weights ω_n, $n = 1, 2, 3$, satisfy the order accuracy condition $\omega_n = \gamma_n + O(h^4)$ [3,6], providing the formal fifth order accuracy to the WENO scheme elaborated in [14,20]. We take $\varepsilon = 10^{-6}$ in our computation.

Remark. For case $(f_i^+)' = 0$, $(f_i^+)'' = 0$, it is also easy to verify that $\omega_n = \gamma_n + O(h^4)$.

Step 5. The new final reconstructions of the numerical flux at $x = x_{i+1/2}$ is given by

$$\hat{f}^+_{i+1/2} = \omega_1\left(\frac{1}{\gamma_1}p_1(x_{i+\frac{1}{2}}) - \frac{\gamma_2}{\gamma_1}p_2(x_{i+\frac{1}{2}}) - \frac{\gamma_3}{\gamma_1}p_3(x_{i+\frac{1}{2}})\right) + \omega_2 p_2(x_{i+\frac{1}{2}}) + \omega_3 p_3(x_{i+\frac{1}{2}}). \tag{2.22}$$

The first term of the right hand side of (2.22) looks very complicated at the first glance. If (2.22) is simply defined as $\omega_1 p_1(x_{i+\frac{1}{2}}) + \omega_2 p_2(x_{i+\frac{1}{2}}) + \omega_3 p_3(x_{i+\frac{1}{2}})$ as usual, the scheme would degrade its optimal fifth order accuracy because of $p_2(x_{i+\frac{1}{2}})$ and $p_3(x_{i+\frac{1}{2}})$ are active and the convex combination together with $p_1(x_{i+\frac{1}{2}})$ would not offer high order approximation at point $x_{i+1/2}$ to numerical flux in smooth region. Thus we should do something to wipe off their contribution in smooth region. By doing so, if a big spatial stencil permits optimal stability and accuracy to be reached, (2.22) could obtain that stability and accuracy obviously. However, when the solution on the big spatial stencil is rough, it is beneficial to seek out smaller two-point TVD-like stencils. Such two small spatial stencils that are used ensure that (when the large five-point spatial stencil may be inactive and ignored) the equation (2.22) can gradually transit to become a TVD scheme with a van Albada-like limiter. So, for the purpose of solving non-smooth numerical solutions, (2.22) performs like a TVD scheme with all the attendant stability properties of a TVD scheme. In this way, it is not very crucial to deliberately choose linear weights for the purpose of sustaining high order accuracy in smooth region and could keep the shock transition sharply in nonsmooth region.

Step 6. The semidiscrete scheme (2.2) is discretized in time by a third order TVD Runge–Kutta method [21]

$$\begin{cases} u^{(1)} &= u^n + \Delta t L(u^n), \\ u^{(2)} &= \frac{3}{4}u^n + \frac{1}{4}u^{(1)} + \frac{1}{4}\Delta t L(u^{(1)}), \\ u^{n+1} &= \frac{1}{3}u^n + \frac{2}{3}u^{(2)} + \frac{2}{3}\Delta t L(u^{(2)}). \end{cases} \tag{2.23}$$

Remark. For the systems of conservation laws, such as the compressible Euler equations, all of the reconstruction procedures are implemented in the local characteristic directions for the purpose of avoiding spurious oscillations. For the two dimensional problems, all of these reconstruction procedures are carried out in a dimension-by-dimension fashion.

3. Numerical tests

In this section we present the results of numerical tests of the fifth order new WENO scheme termed as WENO-ZQ specified in the previous section in comparison to the classical WENO scheme termed as WENO-JS narrated in [14,20] in one and two dimensions. The CFL number is set as 0.6 for WENO-JS and WENO-ZQ schemes in our computations. For the purpose of testing whether the random choice of the linear weights would pollute the optimal order accuracy of WENO-ZQ scheme or not, we set different type of linear weights in the numerical accuracy cases as: (1) $\gamma_1 = 0.98$, $\gamma_2 = 0.01$ and $\gamma_3 = 0.01$; (2) $\gamma_1 = 1.0/3.0$, $\gamma_2 = 1.0/3.0$ and $\gamma_3 = 1.0/3.0$; (3) $\gamma_1 = 0.01$, $\gamma_2 = 0.495$ and $\gamma_3 = 0.495$. And set $\gamma_1 = 0.98$, $\gamma_2 = 0.01$ and $\gamma_3 = 0.01$ in the latter examples.

Example 3.1. We solve the following nonlinear scalar Burgers equation:

$$\mu_t + \left(\frac{\mu^2}{2}\right)_x = 0, \quad 0 < x < 2, \tag{3.1}$$

with the initial condition $\mu(x, 0) = 0.5 + \sin(\pi x)$ and periodic boundary condition. When $t = 0.5/\pi$ the solution is still smooth, and the errors and numerical orders of accuracy by the WENO-ZQ scheme are shown in Table 3.1. For comparison, errors and numerical orders of accuracy by the classical WENO-JS scheme are shown in the same table. We can see that both WENO-ZQ and WENO-JS schemes achieve their designed order of accuracy, and WENO-ZQ scheme with different type of linear weights produces less truncation errors and achieves optimal orders of accuracy. Fig. 3.1 shows that WENO-ZQ scheme needs less CPU time than WENO-JS does to obtain the same quantities of L^1 and L^∞ errors, so WENO-ZQ scheme is more efficient than WENO-JS scheme in this test case.

Example 3.2. We solve the following two-dimensional nonlinear scalar Burgers equation:

$$\mu_t + \left(\frac{\mu^2}{2}\right)_x + \left(\frac{\mu^2}{2}\right)_y = 0, \quad 0 < x, y < 4, \tag{3.2}$$

with the initial condition $\mu(x, y, 0) = 0.5 + \sin(\pi(x + y)/2)$ and periodic boundary conditions. When $t = 0.5/\pi$ the solution is still smooth, and the errors and numerical orders of accuracy by the WENO-ZQ scheme in comparison to that of WENO-JS

Table 3.1
$\mu_t + (\frac{\mu^2}{2})_x = 0$. Initial data $\mu(x,0) = 0.5 + \sin(\pi x)$. WENO-ZQ scheme and WENO-JS scheme. $T = 0.5/\pi$. L^1 and L^∞ errors.

Grid points	WENO-ZQ (1) scheme				WENO-JS scheme			
	L^1 error	Order	L^∞ error	Order	L^1 error	Order	L^∞ error	Order
10	1.64E−2		5.32E−2		1.91E−2		7.48E−2	
20	1.44E−3	3.51	9.73E−3	2.45	2.06E−3	3.21	1.21E−2	2.63
40	7.29E−5	4.31	6.93E−4	3.81	1.24E−4	4.05	1.03E−3	3.54
80	2.38E−6	4.93	3.06E−5	4.50	4.41E−6	4.81	4.72E−5	4.46
160	7.07E−8	5.07	9.31E−7	5.04	1.64E−7	4.75	1.38E−6	5.09
320	2.09E−9	5.07	2.78E−8	5.06	4.76E−9	5.11	7.28E−8	4.25
Grid points	WENO-ZQ (2) scheme				WENO-ZQ (3) scheme			
	L^1 error	Order	L^∞ error	Order	L^1 error	Order	L^∞ error	Order
10	3.48E−2		1.10E−1		3.76E−2		1.16E−1	
20	4.55E−3	2.93	1.55E−2	2.83	5.61E−3	2.74	1.95E−2	2.58
40	1.41E−4	5.01	8.15E−4	4.25	1.68E−4	5.06	1.13E−3	4.11
80	2.57E−6	5.77	3.05E−5	4.74	2.68E−6	5.97	3.04E−5	5.21
160	7.10E−8	5.18	9.31E−7	5.03	7.12E−8	5.23	9.31E−7	5.03
320	2.09E−9	5.08	2.78E−8	5.06	2.09E−9	5.09	2.78E−8	5.06

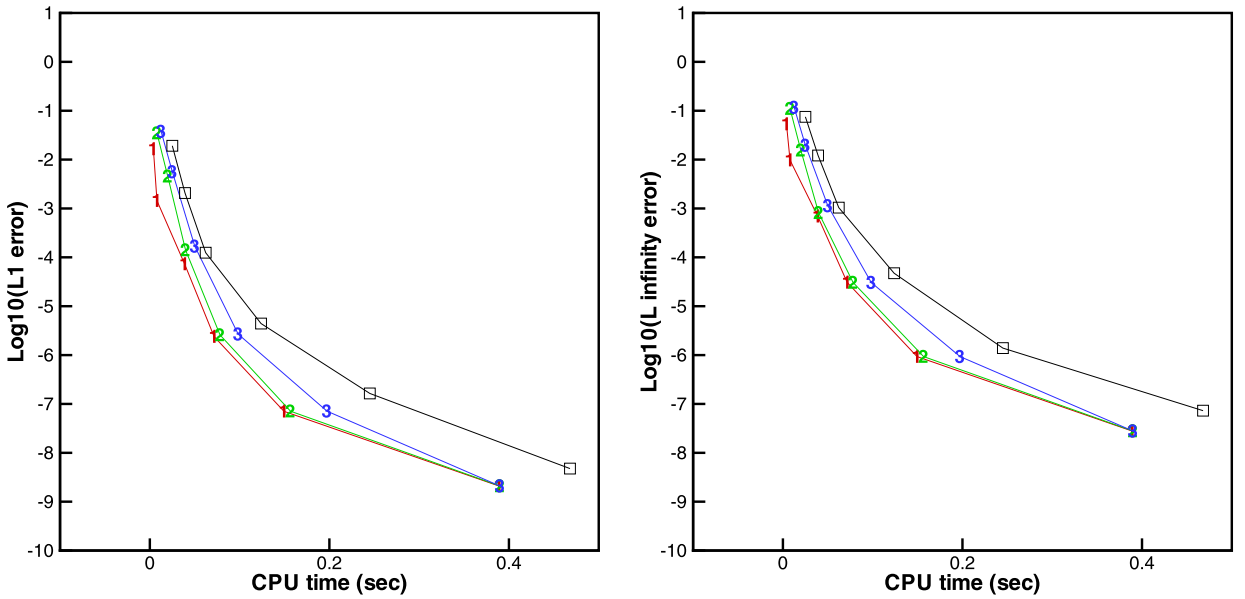

Fig. 3.1. $\mu_t + (\frac{\mu^2}{2})_x = 0$. Initial data $\mu(x,0) = 0.5 + \sin(\pi x)$. Computing time and error. Number signs and a solid red line denote the results of WENO-ZQ scheme with different linear weights (1), (2) and (3); squares and a solid line denote the results of WENO-JS scheme. (For interpretation of the references to color in this figure legend, the reader is referred to the web version of this article.)

scheme are shown in Table 3.2. We can see that the WENO-ZQ scheme with different type of linear weights achieves close to its designed order of accuracy and generates less absolute truncation errors. And the Fig. 3.2 shows that WENO-ZQ scheme needs less CPU time than WENO-JS scheme does to obtain the same quantities of L^1 and L^∞ errors.

Example 3.3.

$$\frac{\partial}{\partial t}\begin{pmatrix}\rho\\ \rho\mu\\ E\end{pmatrix} + \frac{\partial}{\partial x}\begin{pmatrix}\rho\mu\\ \rho\mu^2 + p\\ \mu(E+p)\end{pmatrix} = 0. \tag{3.3}$$

In which ρ is density, μ is the velocity in x-direction, E is total energy and p is pressure. The initial conditions are: $\rho(x,0) = 1 + 0.2\sin(x)$, $\mu(x,0) = 1$, $p(x,0) = 1$, $\gamma = 1.4$. The computing domain is $x \in [0, 2\pi]$. Periodic boundary condition is applied in this test. The exact solution is $\rho(x,t) = 1 + 0.2\sin(x-t)$. The final time is $t = 2$. The errors and numerical orders of accuracy of the density by the WENO-ZQ scheme and WENO-JS scheme are shown in Table 3.3 and the numerical error against CPU time graphs are in Fig. 3.3. We can observe that the theoretical order is actually achieved and the WENO-ZQ scheme can get better results and is more efficient than WENO-JS scheme in this test case.

Table 3.2
$\mu_t + (\frac{\mu^2}{2})_x + (\frac{\mu^2}{2})_y = 0$. Initial data $\mu(x, y, 0) = 0.5 + \sin(\pi(x + y)/2)$. WENO-ZQ scheme and WENO-JS scheme. $T = 0.5/\pi$. L^1 and L^∞ errors.

Grid points	WENO-ZQ (1) scheme				WENO-JS scheme			
	L^1 error	Order	L^∞ error	Order	L^1 error	Order	L^∞ error	Order
10×10	1.84E−2		5.38E−2		2.06E−2		7.49E−2	
20×20	1.73E−3	3.41	9.49E−3	2.50	2.16E−3	3.25	1.21E−2	2.63
40×40	7.46E−5	4.54	6.93E−4	3.78	1.27E−4	4.09	1.03E−3	3.54
80×80	2.41E−6	4.95	3.06E−5	4.50	4.47E−6	4.83	4.72E−5	4.46
160×160	7.11E−8	5.08	9.31E−7	5.04	1.65E−7	4.76	1.38E−6	5.09
320×320	2.09E−9	5.08	2.78E−8	5.06	4.77E−9	5.11	7.28E−8	4.25
Grid points	WENO-ZQ (2) scheme				WENO-ZQ (3) scheme			
	L^1 error	Order	L^∞ error	Order	L^1 error	Order	L^∞ error	Order
10×10	3.81E−2		1.10E−1		4.11E−2		1.17E−1	
20×20	4.82E−3	2.98	1.56E−2	2.82	5.85E−3	2.81	1.92E−2	2.60
40×40	1.42E−4	5.08	7.94E−4	4.30	1.70E−4	5.10	1.10E−3	4.12
80×80	2.61E−6	5.77	3.05E−5	4.70	2.71E−6	5.97	3.04E−5	5.18
160×160	7.14E−8	5.19	9.30E−7	5.03	7.17E−8	5.24	9.30E−7	5.03
320×320	2.09E−9	5.09	2.78E−8	5.06	2.09E−9	5.09	2.78E−8	5.06

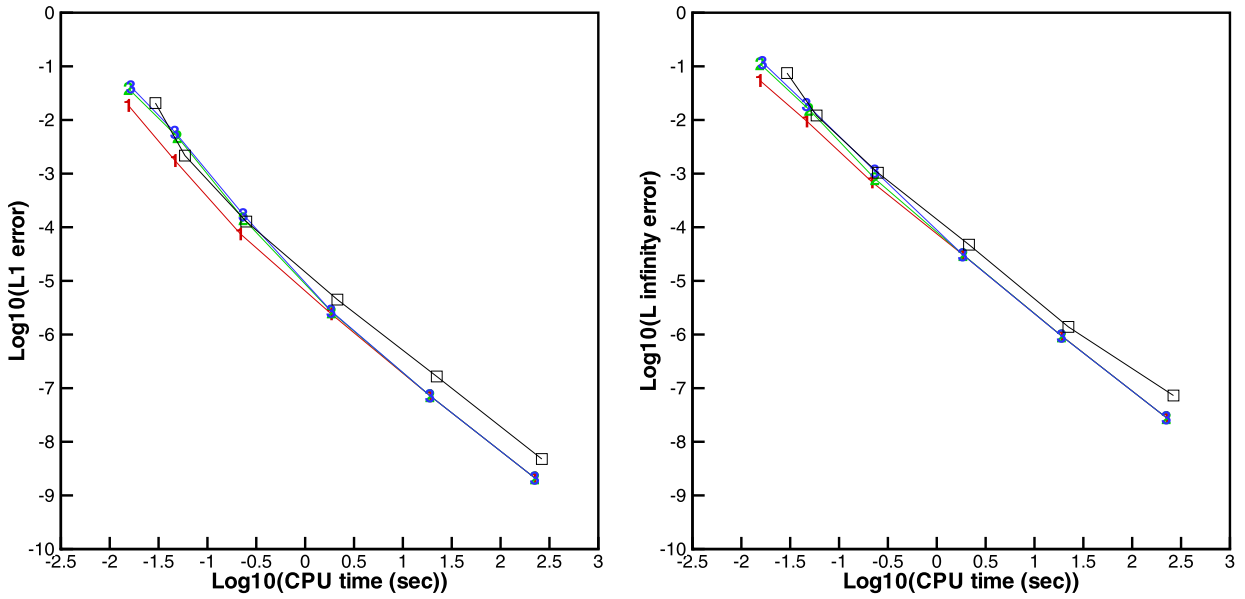

Fig. 3.2. $\mu_t + (\frac{\mu^2}{2})_x + (\frac{\mu^2}{2})_y = 0$. Initial data $\mu(x, y, 0) = 0.5 + \sin(\pi(x + y)/2)$. Computing time and error. Number signs and a solid red line denote the results of WENO-ZQ scheme with different linear weights (1), (2) and (3); squares and a solid line denote the results of WENO-JS scheme. (For interpretation of the references to color in this figure legend, the reader is referred to the web version of this article.)

Table 3.3
1D-Euler equations: initial data $\rho(x, 0) = 1 + 0.2\sin(x)$, $\mu(x, 0) = 1$ and $p(x, 0) = 1$. WENO-ZQ scheme and WENO-JS scheme. $T = 2$. L^1 and L^∞ errors.

Grid points	WENO-ZQ (1) scheme				WENO-JS scheme			
	L^1 error	Order	L^∞ error	Order	L^1 error	Order	L^∞ error	Order
10	1.36E−3		3.51E−3		4.49E−3		6.79E−3	
20	3.04E−5	5.49	5.97E−5	5.87	2.15E−4	4.38	3.75E−4	4.18
40	9.62E−7	4.98	1.60E−6	5.21	6.74E−6	5.00	1.28E−5	4.87
80	3.01E−8	5.00	4.75E−8	5.07	2.07E−7	5.02	3.99E−7	5.01
160	9.39E−10	5.00	1.47E−9	5.01	6.38E−9	5.02	1.15E−8	5.11
320	2.93E−11	5.00	4.60E−11	5.00	1.92E−10	5.05	3.16E−10	5.19
Grid points	WENO-ZQ (2) scheme				WENO-ZQ (3) scheme			
	L^1 error	Order	L^∞ error	Order	L^1 error	Order	L^∞ error	Order
10	8.59E−3		2.27E−2		1.08E−2		2.70E−2	
20	1.30E−4	6.05	3.98E−4	5.84	1.88E−4	5.85	5.31E−4	5.67
40	9.98E−7	7.02	5.07E−6	6.29	1.15E−6	7.34	6.80E−6	6.28
80	3.01E−8	5.05	6.48E−8	6.29	3.01E−8	5.27	7.35E−8	6.53
160	9.39E−10	5.00	1.54E−9	5.39	9.39E−10	5.00	1.58E−9	5.53
320	2.93E−11	5.00	4.60E−11	5.07	2.93E−11	5.00	4.61E−11	5.10

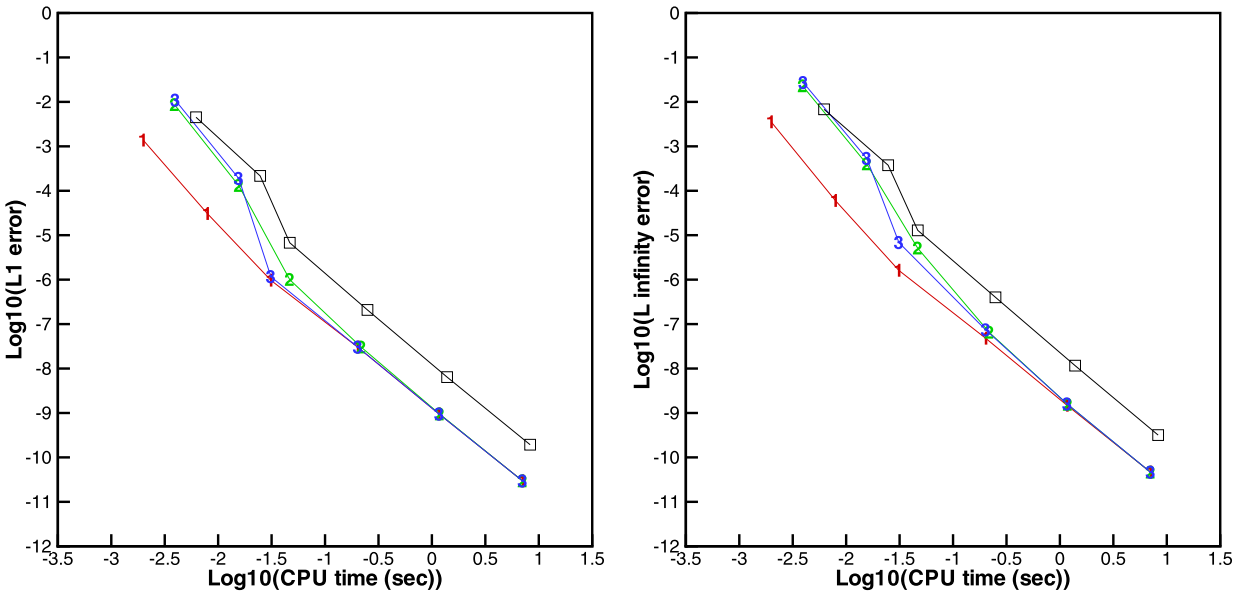

Fig. 3.3. 1D-Euler equations: initial data $\rho(x,0)=1+0.2\sin(x)$, $\mu(x,0)=1$ and $p(x,0)=1$. Computing time and error. Number signs and a solid red line denote the results of WENO-ZQ scheme with different linear weights (1), (2) and (3); squares and a solid line denote the results of WENO-JS scheme. (For interpretation of the references to color in this figure legend, the reader is referred to the web version of this article.)

Table 3.4
2D-Euler equations: initial data $\rho(x,y,0)=1+0.2\sin(x+y)$, $\mu(x,y,0)=1$, $\nu(x,y,0)=1$ and $p(x,y,0)=1$. WENO-ZQ scheme and WENO-JS scheme. $T=2$. L^1 and L^∞ errors.

Grid points	WENO-ZQ (1) scheme				WENO-JS scheme			
	L^1 error	Order	L^∞ error	Order	L^1 error	Order	L^∞ error	Order
10×10	6.32E−4		1.00E−3		3.68E−3		7.51E−3	
20×20	1.74E−5	5.18	3.15E−5	5.00	1.37E−4	4.75	2.57E−4	4.87
40×40	5.01E−7	5.11	9.31E−7	5.08	3.62E−6	5.24	6.63E−6	5.28
80×80	1.49E−8	5.07	2.81E−8	5.05	9.47E−8	5.25	1.78E−7	5.22
160×160	4.56E−10	5.04	8.62E−10	5.03	2.40E−9	5.30	4.74E−9	5.23
320×320	1.40E−11	5.02	2.66E−11	5.01	5.56E−11	5.43	1.12E−10	5.39
Grid points	WENO-ZQ (2) scheme				WENO-ZQ (3) scheme			
	L^1 error	Order	L^∞ error	Order	L^1 error	Order	L^∞ error	Order
10×10	1.44E−3		3.59E−3		1.90E−3		4.48E−3	
20×20	1.86E−5	6.28	3.37E−5	6.74	1.93E−5	6.62	3.94E−5	6.83
40×40	5.03E−7	5.21	9.25E−7	5.19	5.04E−7	5.26	9.24E−7	5.41
80×80	1.49E−8	5.07	2.81E−8	5.04	1.49E−8	5.07	2.81E−8	5.04
160×160	4.56E−10	5.04	8.62E−10	5.03	4.56E−10	5.04	8.62E−10	5.03
320×320	1.40E−11	5.02	2.66E−11	5.01	1.40E−11	5.02	2.66E−11	5.01

Example 3.4.

$$\frac{\partial}{\partial t}\begin{pmatrix}\rho\\ \rho\mu\\ \rho\nu\\ E\end{pmatrix}+\frac{\partial}{\partial x}\begin{pmatrix}\rho\mu\\ \rho\mu^2+p\\ \rho\mu\nu\\ \mu(E+p)\end{pmatrix}+\frac{\partial}{\partial y}\begin{pmatrix}\rho\nu\\ \rho\mu\nu\\ \rho\nu^2+p\\ \nu(E+p)\end{pmatrix}=0. \tag{3.4}$$

In which ρ is density; μ and ν are the velocities in the x and y-directions, respectively; E is total energy; and p is pressure. The initial conditions are: $\rho(x,y,0)=1+0.2\sin(x+y)$, $\mu(x,y,0)=1$, $\nu(x,y,0)=1$, $p(x,y,0)=1$ and $\gamma=1.4$. The computing domain is $(x,y)\in[0,2\pi]\times[0,2\pi]$. Periodic boundary conditions are applied in both directions. The exact solution is $\rho(x,y,t)=1+0.2\sin(x+y-2t)$. We compute the solution up to $t=2$. The errors and numerical orders of accuracy of the density by the WENO-ZQ scheme and WENO-JS scheme are shown in Table 3.4 and the numerical error against CPU time graphs are in Fig. 3.4. WENO-ZQ scheme with different type of linear weights is better than WENO-JS scheme in this two dimensional test case.

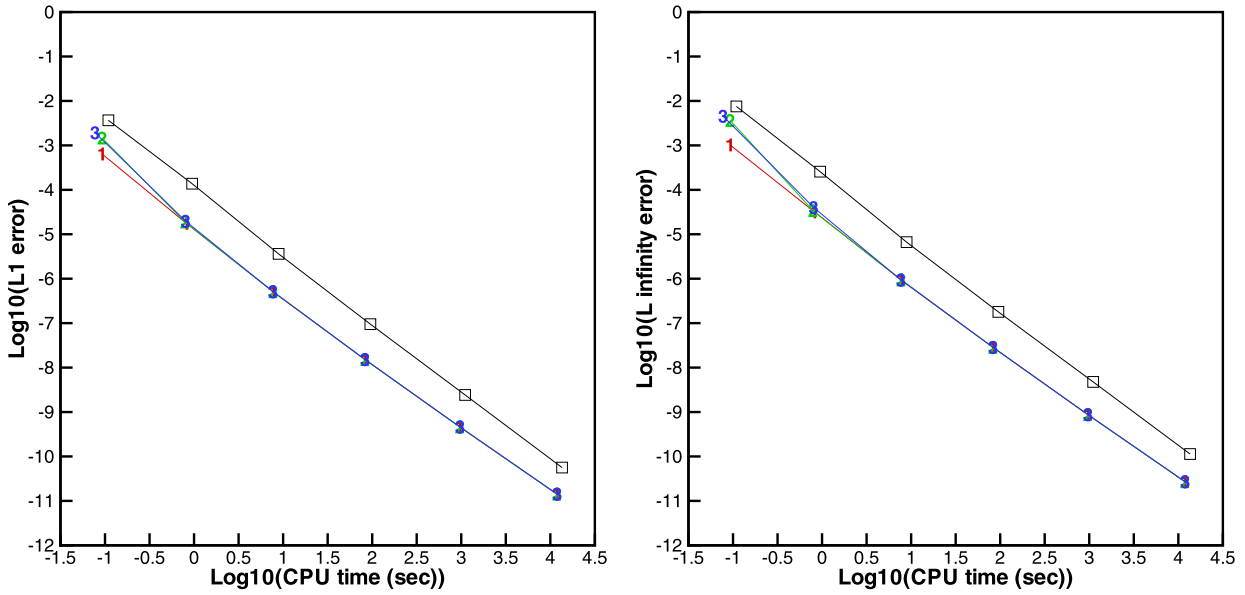

Fig. 3.4. 2D-Euler equations: initial data $\rho(x, y, 0) = 1 + 0.2\sin(x + y)$, $\mu(x, y, 0) = 1$, $\nu(x, y, 0) = 1$ and $p(x, y, 0) = 1$. Computing time and error. Number signs and a solid red line denote the results of WENO-ZQ scheme with different linear weights (1), (2) and (3); squares and a solid line denote the results of WENO-JS scheme. (For interpretation of the references to color in this figure legend, the reader is referred to the web version of this article.)

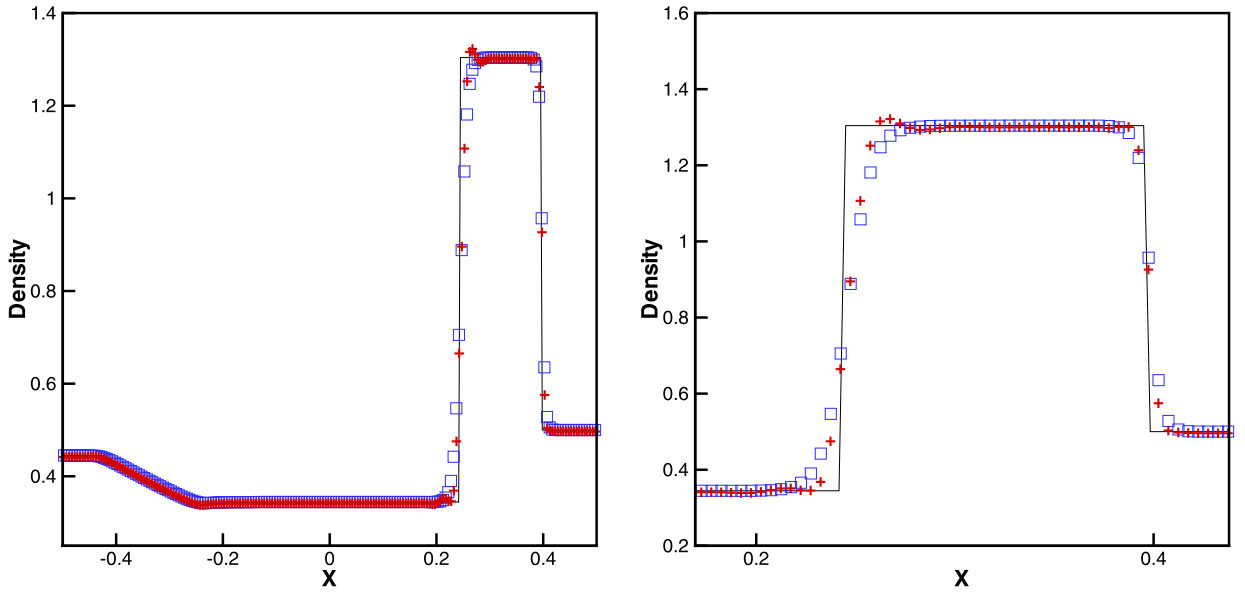

Fig. 3.5. The Lax problem. $T = 0.16$. From left to right: density; density zoomed in. Solid line: the exact solution; plus signs: the results of WENO-ZQ scheme; squares: the results of WENO-JS scheme. Grid points: 200.

Example 3.5. We solve the 1D Euler equations with Riemann initial condition for the Lax problem:

$$(\rho, u, p, \gamma)^T = \begin{cases} (0.445, 0.698, 3.528, 1.4)^T, & x \in [-0.5, 0), \\ (0.5, 0, 0.571, 1.4)^T, & x \in [0, 0.5]. \end{cases} \tag{3.5}$$

For $t = 0.16$, we present in Fig. 3.5 the exact solution and the computed density ρ obtained with the WENO-ZQ scheme comparing to the WENO-JS scheme by using 200 grid points. The results and zoomed in picture for different schemes are shown in Fig. 3.5. We observe that the computational results obtained by the WENO-ZQ scheme works better than the WENO-JS scheme.

Example 3.6. A higher order scheme would show its advantage when the solution contains both shocks and complex smooth region structures. A typical example for this is the problem of shock interaction with entropy waves [20]. We

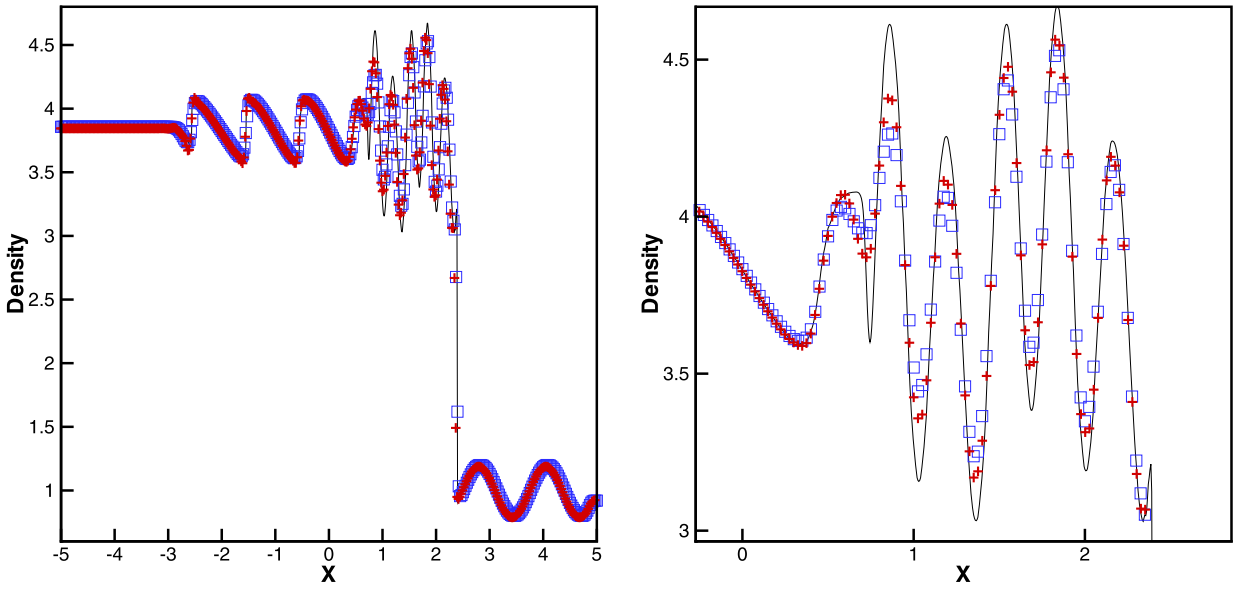

Fig. 3.6. The shock density wave interaction problem. $T = 1.8$. From left to right: density; density zoomed in. Solid line: the exact solution; plus signs: the results of WENO-ZQ scheme; squares: the results of WENO-JS scheme. Grid points: 400.

solve the Euler equations (3.3) with a moving Mach = 3 shock interacting with sine waves in density: $(\rho, \mu, p, \gamma)^T = (3.857143, 2.629369, 10.333333, 1.4)^T$ for $x \in [-5, -4)$; $(\rho, \mu, p, \gamma)^T = (1 + 0.2\sin(5x), 0, 1, 1.4)^T$ for $x \in [-4, 5]$. The computed density ρ is plotted at t = 1.8 against the referenced "exact" solution which is a converged solution computed by the finite difference fifth order WENO scheme [14] with 2000 grid points in Fig. 3.6. The results and zoomed in picture for different schemes are also shown in Fig. 3.6. The WENO-ZQ scheme could get much better resolution than that of WENO-JS scheme.

Example 3.7. We now consider the interaction of two blast waves. The initial conditions are:

$$(\rho, u, p, \gamma)^T = \begin{cases} (1, 0, 10^3, 1.4)^T, & 0 < x < 0.1, \\ (1, 0, 10^{-2}, 1.4)^T, & 0.1 < x < 0.9, \\ (1, 0, 10^2, 1.4)^T, & 0.9 < x < 1. \end{cases} \tag{3.6}$$

The computed density ρ is plotted at $t = 0.038$ against the reference "exact" solution which is a converged solution computed by the finite difference fifth order WENO scheme [14] with 20000 grid points in Fig. 3.7. The results and zoomed in picture for different schemes are shown in Fig. 3.7.

Example 3.8. Double Mach reflection problem [24]. We solve the Euler equations (3.4) in a computational domain of $[0, 4] \times [0, 1]$. A reflection wall lies at the bottom of the domain starting from $x = \frac{1}{6}$, $y = 0$, making a 60^o angle with the x-axis. The reflection boundary condition is used at the wall, which for the rest of the bottom boundary (the part from $x = 0$ to $x = \frac{1}{6}$), the exact post-shock condition is imposed. At the top boundary is the exact motion of the Mach 10 shock and $\gamma = 1.4$. The results are shown at $t = 0.2$. We present the pictures of region $[0, 3] \times [0, 1]$ and the blow-up region around the double Mach stems in Fig. 3.8. The WENO-ZQ scheme could gain better density resolutions than the same order WENO-JS scheme.

Example 3.9. A Mach 3 wind tunnel with a step. This model problem is also originally from [24]. The setup of the problem is as follows. The wind tunnel is one length unit wide and three length units long. The step is 0.2 length units high and is located 0.6 length units from the left-hand end of the tunnel. The problem is initialized by a right-going Mach 3 flow. Reflective boundary conditions are applied along the wall of the tunnel and inflow/outflow boundary conditions are applied at the entrance/exit. The results are shown at $t = 4$. In Fig. 3.9, we show 30 equally spaced density contours from 0.32 to 6.15 computed by the WENO-ZQ scheme comparing with WENO-JS scheme. We can clearly observe that the different schemes give good resolution especially for the resolution of the physical instability and roll-up of the contact line.

Remark. We can also use the same methodology to obtain higher order new WENO-ZQ schemes such as the seventh order and ninth order WENO-ZQ schemes. Although such new schemes would sustain their optimal order accuracy in smooth region, they could not give more sharp shock transitions than the proposed fifth order accurate WENO-ZQ scheme. If the big spatial stencil contains discontinuities, the high degree polynomial defined on it is inactive and at least one of the two

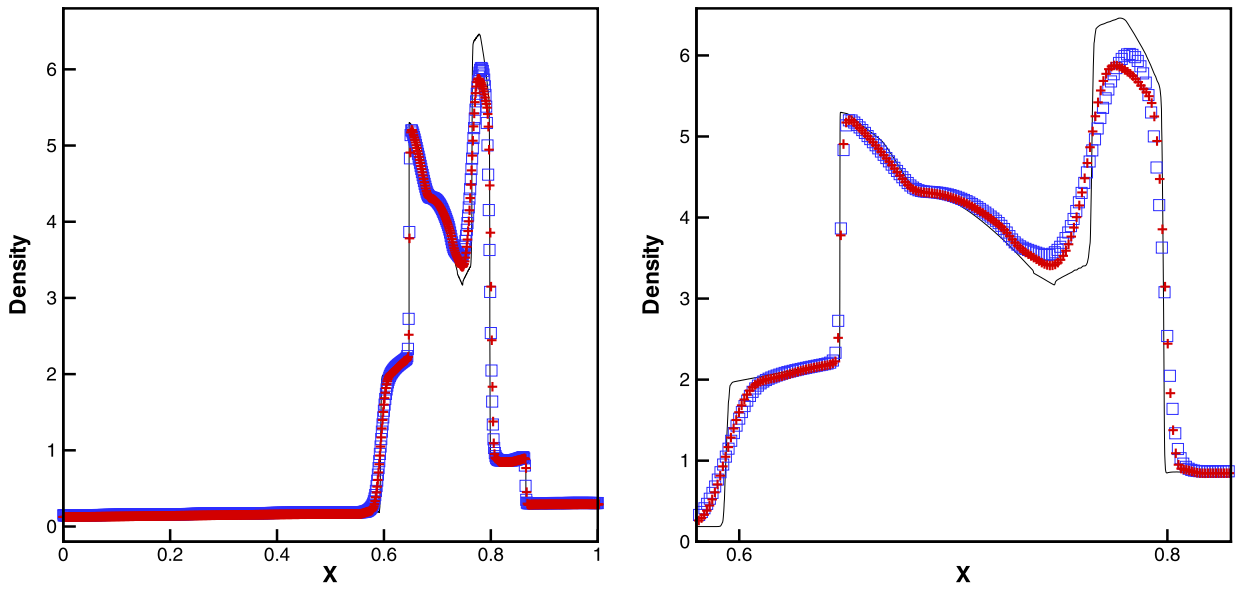

Fig. 3.7. The blast wave problem. $T = 0.038$. From left to right: density; density zoomed in. Solid line: the exact solution; plus signs: the results of WENO-ZQ scheme; squares: the results of WENO-JS scheme. Grid points: 800.

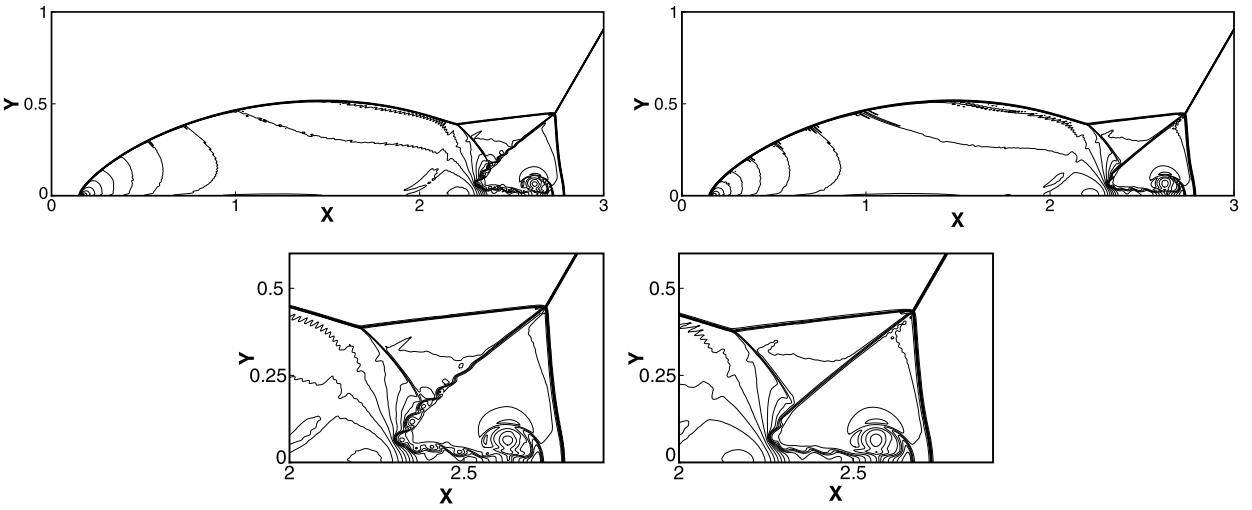

Fig. 3.8. Double Mach reflection problem. $T = 0.2$, with grid points: 1600×400. 30 equally spaced density contours from 1.5 to 22.7. Zoom-in pictures around the Mach stem (Bottom). WENO-ZQ scheme (left); WENO-JS scheme (right).

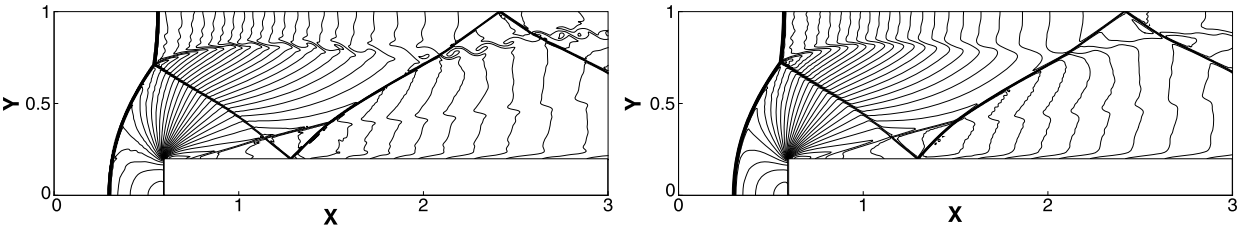

Fig. 3.9. Forward step problem. $T = 4.0$, with grid points: 600×200. 30 equally spaced density contours from 0.32 to 6.15. WENO-ZQ scheme (left); WENO-JS scheme (right).

linear polynomials is valid and results in the scheme degrades to second order accuracy adjacent to discontinuous region. The more we use wilder spatial stencil, the bigger probability of the scheme degrades to lower order accuracy. So it is reasonable for us to draw the conclusion that the fifth order WENO-ZQ scheme gets better resolutions than higher order WENO-ZQ schemes in nonsmooth region.

4. Concluding remarks

In this paper a new simple finite difference fifth order WENO scheme termed as WENO-ZQ is constructed for solving the hyperbolic conservation laws. The crucial advantages of WENO-ZQ scheme are its simplicity and simultaneously obtaining optimal fifth order accuracy with three unequal spatial stencils. By the usage of information lies in the five-point and two smaller two-point spatial stencils, the procedure of this new WENO methodology is adopted by artificially setting linear weights for conservation, computing associated smoothness indicators and redefining new nonlinear weights which are different to the formula narrated in [3,6] etc. The constructions of such WENO-ZQ scheme are based on WENO interpolation in spatial field and then the third order TVD Runge–Kutta time discretization procedure is used for solving the ODE. In WENO-ZQ scheme, the nodal point information is used via time approaching and is easier to be implemented than the classical finite difference WENO scheme [14,20]. Comparing it with the classical WENO schemes [14,20], the WENO-ZQ scheme is very simple in the computation of problems with strong shocks, can obtain the same order accuracy in the same big stencil simultaneously having less absolute numerical truncation errors in L^1 and L^∞ norms. Extensive numerical experiments for compressible Euler systems of gas dynamics are presented to show the simplicity and effectiveness of this WENO-ZQ scheme.

The procedure of this new WENO reconstruction can be easily extended to finite volume version, and it will be more efficient and simpler than the current finite volume WENO schemes, especially for methods on unstructured meshes. The research is going on.

References

[1] D.S. Balsara, T. Rumpf, M. Dumbser, C.D. Munz, Efficient, high accuracy ADER–WENO schemes for hydrodynamics and divergence-free magnetohydrodynamics, J. Comput. Phys. 228 (2009) 2480–2516.
[2] D.S. Balsara, C.-W. Shu, Monotonicity preserving weighted essentially non-oscillatory schemes with increasingly high order of accuracy, J. Comput. Phys. 160 (2000) 405–452.
[3] R. Borges, M. Carmona, B. Costa, W.S. Don, An improved weighted essentially non-oscillatory scheme for hyperbolic conservation laws, J. Comput. Phys. 227 (2008) 3191–3211.
[4] J. Casper, Finite-volume implementation of high-order essentially nonoscillatory schemes in two dimensions, AIAA J. 30 (1992) 2829–2835.
[5] J. Casper, H.L. Atkins, A finite-volume high-order ENO scheme for two-dimensional hyperbolic systems, J. Comput. Phys. 106 (1993) 62–76.
[6] M. Castro, B. Costa, W.S. Don, High order weighted essentially non-oscillatory WENO-Z schemes for hyperbolic conservation laws, J. Comput. Phys. 230 (2011) 1766–1792.
[7] M. Dumbser, M. Käser, Arbitrary high order non-oscillatory finite volume schemes on unstructured meshes for linear hyperbolic systems, J. Comput. Phys. 221 (2007) 693–723.
[8] A. Harten, High resolution schemes for hyperbolic conservation laws, J. Comput. Phys. 49 (3) (1983) 357–393.
[9] A. Harten, Preliminary results on the extension of ENO schemes to two-dimensional problems, in: C. Carasso, et al. (Eds.), Proceedings, International Conference on Nonlinear Hyperbolic Problems, Saint-Etienne, 1986, in: Lecture Notes in Mathematics, Springer-Verlag, Berlin, 1987.
[10] A. Harten, B. Engquist, S. Osher, S. Chakravarthy, Uniformly high order accurate essentially non-oscillatory schemes III, J. Comput. Phys. 71 (1987) 231–323.
[11] A. Harten, S. Osher, Uniformly high-order accurate non-oscillatory schemes, IMRC Technical Summary Rept. 2823, Univ. of Wisconsin, Madison, WI, May 1985.
[12] G. Hu, R. Li, T. Tang, A robust WENO type finite volume solver for steady Euler equations on unstructured grids, Commun. Comput. Phys. 9 (2011) 627–648.
[13] C. Hu, C.-W. Shu, Weighted essentially non-oscillatory schemes on triangular meshes, J. Comput. Phys. 150 (1999) 97–127.
[14] G.-S. Jiang, C.-W. Shu, Efficient implementation of weighted ENO schemes, J. Comput. Phys. 126 (1996) 202–228.
[15] X.D. Liu, S. Osher, T. Chan, Weighted essentially non-oscillatory schemes, J. Comput. Phys. 115 (1994) 200–212.
[16] Y. Liu, Y.T. Zhang, A robust reconstruction for unstructured WENO schemes, J. Sci. Comput. 54 (2013) 603–621.
[17] S. Pirozzoli, Conservative hybrid compact-WENO schemes for shock–turbulence interaction, J. Comput. Phys. 178 (2002) 81–117.
[18] Y.Q. Shen, G.W. Yang, Hybrid finite compact-WENO schemes for shock calculation, Int. J. Numer. Methods Fluids 53 (2007) 531–560.
[19] Y.Q. Shen, G.C. Zha, A robust seventh-order WENO scheme and its applications, 46th AIAA Aerospace Sciences Meeting and Exhibit, Reno, Nevada, AIAA 2008-757, 2008.
[20] C.-W. Shu, High order weighted essentially nonoscillatory schemes for convection dominated problems, SIAM Rev. 51 (2009) 82–126.
[21] C.-W. Shu, S. Osher, Efficient implementation of essentially non-oscillatory shock capturing schemes, J. Comput. Phys. 77 (1988) 439–471.
[22] C.-W. Shu, S. Osher, Efficient implementation of essentially non-oscillatory shock capturing schemes, II, J. Comput. Phys. 83 (1989) 32–78.
[23] Z.J. Wang, R.F. Chen, Optimized weighted essentially non-oscillatory schemes for linear waves with discontinuity, J. Comput. Phys. 174 (2001) 381–404.
[24] P. Woodward, P. Colella, The numerical simulation of two-dimensional fluid flow with strong shocks, J. Comput. Phys. 54 (1984) 115–173.
[25] Y.T. Zhang, C.-W. Shu, Third order WENO scheme on three dimensional tetrahedral meshes, Commun. Comput. Phys. 5 (2009) 836–848.
[26] X. Zhong, C.-W. Shu, A simple weighted essentially nonoscillatory limiter for Runge–Kutta discontinuous Galerkin methods, J. Comput. Phys. 232 (2013) 397–415.